A non-normal mode marginal state of convection in a porous rectangle

Peder A. Tyvand · Jonas Kristiansen Nøland · Leiv Storesletten

Received: date / Accepted: date

Abstract The 4th order Darcy-Bénard eigenvalue problem for onset of thermal convection in a 2D rectangular porous box is investigated. The conventional type of solution has normal-mode dependency in at least one of the two spatial directions. The present eigenfunctions are of non-normal mode type both in the horizontal and the vertical direction. A numerical solution is found by the finite element method, since no analytical method is known for this non-degenerate fourth-order eigenvalue problem. All four boundaries of the rectangle are impermeable. The thermal conditions are hand-picked to be incompatible with normal modes: The lower boundary and the right-hand wall are heat conductors. The upper boundary has given heat flux. The left-hand wall is thermally insulating. The computed eigenfunctions have novel types of complicated cell structures, with intricate internal cell walls.

1 Introduction

The onset of convection in a horizontal porous layer was first studied by Horton and Rogers (1945) and Lapwood (1948). The reputation of this HRL problem

P. A. Tyvand
Faculty of Mathematical Sciences and Technology
Norwegian University of Life Sciences
1432 Ås, Norway
Tel.: +47-67231564
E-mail: Peder.Tyvand@nmbu.no

J. K. Nøland
Faculty of Information Technology and Electrical Engineering
Norwegian University of Science and Technology
E-mail: Jonas.K.Noland@ntnu.no

L. Storesletten
Department of Mathematics
University of Agder
E-mail: Leiv.Storesletten@uia.no

is that it is the simplest mathematical problem of thermomechanical instability. Still there are mathematical challenges, especially those related to the fact that the eigenvalue problem is of fourth order in space. Since the biharmonic operator does not separate in orthogonal coordinate systems, there is no general closed-form analytical eigenfunction available, even for a rectangular geometry.

In the literature on the HRL eigenvalue problem, the boundary conditions have tacitly been restricted to make analytical solutions possible. Wooding (1959) circumvented the restrictions of the non-separability of the biharmonic operator for vertical porous cylinders, by a normal-mode assumption that restricted the cylinder wall conditions to be equivalent to internal cell walls. Tyvand and Storesletten (2018) verified Wooding's normal-mode assumption from first principles.

A normal mode is the spatial dependency of free vibrations according to the linear wave equation. Inserting the time dependency of a single oscillatory frequency changes the wave equation to a Helmholtz eigenvalue equation for the free vibrations, with the wave number as the eigenvalue. This is the equation valid for free vibrations of strings in 1D, of elastic membranes in 2D and for sound waves in 3D. Normal modes are thus linked to differential equations that are of second order in space, where any choice of homogeneous boundary conditions may fit automatically. This is not the case for higher-order systems, where the full set of independent boundary conditions prevents the general validity of normal modes. Still the normal modes are in common use for analytical eigenfunctions of higher-order systems. This can only be justified by applying degenerate boundary conditions, as was demonstrated by Wooding (1959) for convection in a vertical porous cylinder. The details of Wooding's theory were carried out by Beck (1972) and Zebib (1978), for rectangular and circular cylinders, respectively.

With normal modes valid over the horizontal cylinder cross-section, there is no need for normal modes in the third (vertical) direction in order to derive analytical eigenfunctions. This fact was demonstrated by Nield (1968, Appendix), who solved all the Dirichlet and Neumann type fourth-order problems onset of convection in a porous medium between two horizontal planes. Wang (1998, 1999) exemplified how the cases solved by Nield (1968) can be adjusted to be valid for cylinders with with normal-mode compatible wall conditions. The wave number in Nield's solutions will then appear as the eigenvalue of the Helmholtz equation that applies to the cross-section of the cylinder. There are two classes of normal-mode compatible eigenvalue problems for cylinders: The Neumann type of impermeable/insulating conditions (Wooding 1959) and Dirichlet type of conducting walls that are open to inflow/outflow. Barletta and Storesletten (2015) solved the cylinder problem with these Dirichlet conditions, both for a circular cross-section and an elliptical cross-section.

Non-normal modes in the horizontal direction is an interesting possibility that was first explored by Nilsen and Storesletten (1990). Lyubimov (1975) had suggested but not derived such solutions. To solve the problem analytically requires normal modes in the vertical direction, following Horton and

Rogers (1945). A non-normal mode solution for a full 3D problem was given by Haugen and Tyvand (2003), for a circular cylinder with conducting walls. In the tangential direction, continuity and periodicity gives normal modes in terms of the azimuthal angle coordinate. Again the analysis rested on normal modes in the vertical direction.

What will happen to the HRL eigenvalue problem for a rectangular box when the set of boundary conditions fails to be compatible with normal modes, in the horizontal as well as in the vertical direction? This is the topic of the present paper, and for simplicity we consider only a 2D rectangular box. We hand-pick the boundary conditions so that two out of four boundaries have conditions that are compatible with normal modes, only to be overruled by the other boundaries that prevent normal modes from contributing to the solution. The resulting eigenfunction is a fully non-normal mode solution in 2D, and it can only be determined numerically, since no analytical methods are known.

When we study non-normal mode convection cells, we search for qualitative features of the cells: The shapes of the internal cell walls, the recirculation patterns and the relationships between streamlines and isotherms. We expect more complicated cell patterns than the well-known HRL cell, which has a full normal-mode type sinusoidal spatial dependency.

Earlier analytical work on the onset of convection in homogeneous and isotropic porous rectangles has not been able to identify flow cells that have irregular curved shapes of the internal cell walls. A tacit assumption has been a normal-mode type of behavior either in the horizontal or vertical direction. Thereby the cells are forced to have vertical internal cell walls, as well as horizontal internal cell walls when higher vertical modes are taken into consideration. The literature on the topic tends to assume that internal cell walls in a marginal linearized state of convection onset in 2D rectangular porous rectangles will always have rectangular internal cell walls, parallel to the external rectangular boundaries. However, this assumption has has never been proven, and in the present paper we will demonstrate that it is incorrect.

In linearized theory of convection onset, one looks for the critical Rayleigh number and the corresponding preferred cell width. The present numerical solutions will produce precise Rayleigh numbers, but there will be no precise concept of cell width. The shapes of the internal flow cells and thermal cells will differ from one another, and their internal cell walls may have complicated curved shapes that defy the wave number concept.

2 Mathematical formulation

A porous medium is considered, with 2D flow in the x, z plane. Physically this corresponds to a 3D porous medium with impermeable and insulating walls $y = 0$ and $y = b$, where the distance b is sufficiently small compared with the vertical length scale, implying that the preferred mode of free convection will be 2D. The z axis is directed vertically upwards. The porous medium is homogeneous and isotropic. The assumption of 2D flow in the x, z plane is

valid also for a 3D porous medium with thickness b in the y direction, if two constraints are met: (i) The thermomechanical wall conditions at $y = 0$ and $y = b$ are those of impermeable and thermally insulating walls. (ii) The cell width in the x direction must be sufficiently large compared with b.

From now on we assume these conditions for 2D flow in the x, z plane to be met without specifying them further. Storesletten and Tveitereid (1991) investigated a problem where the range of validity of this assumption of 2D flow has been scrutinized.

The velocity vector $\mathbf{v}$ has Cartesian components (u, w). The temperature field is $T(x, z, t)$, with t denoting time. The undisturbed motionless state has uniform vertical temperature gradient. The gravitational acceleration g is written in vector form as $\mathbf{g}$.

The standard Darcy-Boussinesq equations for convection in a homogeneous and isotropic porous medium can be written

$$\nabla p + \frac{\mu}{K}\mathbf{v} + \rho_0\beta\ (T - T_0)\mathbf{g} = 0, \tag{1}$$

$$\nabla \cdot \mathbf{v} = 0, \tag{2}$$

$$(\rho c_p)_m \frac{\partial T}{\partial t} + (\rho c_p)_f\ \mathbf{v} \cdot \nabla T = \lambda_m \nabla^2 T. \tag{3}$$

In these equations, p is the dynamic pressure, β is the coefficient of thermal expansion, $\rho = \rho_0$ is the fluid density at the reference temperature T_0, μ is the dynamic viscosity of the saturating fluid, K is the permeability, c_p is the specific heat at constant pressure, and λ_m is the thermal conductivity of the saturated porous medium. The subscript m refers to an average over the solid/fluid mixture, while the subscript f refers to the saturating fluid alone.

We consider a 2D porous medium with a rectangular shape, bounded by the four sides

$$x = 0, \quad x = l, \quad z = 0, \quad z = h. \tag{4}$$

The lower boundary is taken to be impermeable and perfectly heat-conducting

$$w = 0, \quad T - T_0 = 0, \quad \text{at} \quad z = 0, \tag{5}$$

while the upper boundary is taken to be impermeable and with constant uniform heat flux

$$w = 0, \quad \frac{\partial T}{\partial z} = -\frac{\Delta T}{h}, \quad \text{at} \quad z = h, \tag{6}$$

where ΔT is the temperature difference across the layer in its undisturbed state. T_0 is a reference temperature The left-hand boundary is assumed to be impermeable and thermally insulating

$$u = 0, \quad \frac{\partial T}{\partial x} = 0, \quad \text{at} \quad x = 0, \tag{7}$$

while the right-hand boundary is assumed to be impermeable and perfectly conducting

$$u = 0, \quad T - T_0 = -\frac{\Delta T}{h} z, \quad \text{at} \quad x = l. \tag{8}$$

These four boundary conditions are hand-picked to violate in a mild way the requirements for normal mode solutions, both in the horizontal and the vertical direction. These conditions are designed to be as simple as possible. The lower and the left-hand boundary condition alone are in themselves compatible with normal modes. The violation of normal modes is due to the upper boundary condition as far as the vertical dependency of the eigenfunction is concerned. The violation of normal modes in due to the right-hand boundary condition as far as the horizontal dependency is concerned.

The upper right-hand corner (l, h) is thus the troublesome corner where two non-normal mode type of conditions meet. Not surprising, we will discover small convergence problems near the upper-right hand corner, and we will apply a finer numerical grid around this corner than elsewhere in the rectangular fluid domain.

2.1 Dimensionless equations

From now on we work with dimensionless variables. We reformulate the mathematical problem in dimensionless form by means of the transformations

$$\begin{gathered}\frac{1}{h}(x,z)\to(x,z),\qquad \frac{h}{\kappa_m}(u,w)\to(u,w),\qquad h\nabla\to\nabla,\\ \frac{1}{\Delta T}(T-T_0)\to T,\qquad \frac{K}{\mu\kappa_m}(p-p_0)\to p,\qquad \frac{(\rho c_p)_f\kappa_m}{(\rho c_p)_m H^2}t\to t,\end{gathered}\tag{9}$$

where $\kappa_m = \lambda_m/(\rho_0 c_p)_f$ is the thermal diffusivity of the saturated porous medium. We denote the vertical unit vector by $\mathbf{k}$, directed upwards.

The dimensionless governing equations can then be written

$$\mathbf{v} + \nabla p - R\,T\mathbf{k} = 0. \tag{10}$$

$$\nabla\cdot\mathbf{v} = 0 \tag{11}$$

$$\frac{\partial T}{\partial t} + \mathbf{v}\cdot\nabla T = \nabla^2 T, \tag{12}$$

with the boundary conditions at the lower and upper boundaries

$$w = T = 0, \quad z = 0, \tag{13}$$

$$w = \frac{\partial T}{\partial z} + 1 = 0, \quad z = 1. \tag{14}$$

The boundary conditions at the sidewalls are

$$\frac{\partial T}{\partial x} = u = 0, \quad x = 0, \tag{15}$$

$$T = u = 0, \quad x = l/h. \tag{16}$$

We have introduced the Rayleigh number R defined as

$$R = \frac{\rho_0 g\beta K\Delta T h}{\mu\kappa_m}. \tag{17}$$

2.2 Basic solution

The stationary basic solution of eqs. (10)-(14) is given subscript "b"

$$\mathbf{v}_b = 0, \quad T_b = -z, \quad p_b = -\frac{1}{2} R \, z^2. \tag{18}$$

This basic state of hydrostatic fluid has a linear temperature profile.

2.3 Linearized perturbation equations

In our stability analysis we disturb the static state (18) with perturbed fields

$$\mathbf{v} = \mathbf{v}_b + \mathbf{v}, \quad T = T_b(z) + \theta, \quad p = p_b(z) + p'. \tag{19}$$

with perturbations $\mathbf{v}, \theta, p'$ that are functions of x, z and t. Linearizing eqs. (10)-(12) with respect to perturbations and eliminating the pressure gives

$$\nabla^2 w = R \frac{\partial^2 \theta}{\partial x^2}, \tag{20}$$

$$\frac{\partial \theta}{\partial t} - w = \nabla^2 \theta. \tag{21}$$

The onset of convection is assumed to occur with a steady (non-oscillatory) marginal state. The only known case where the present configuration of a porous rectangular box is known to give a advected wave solution at marginal stability, was investigated by Rees and Tyvand (2004a). Here the two vertical end-walls were mutually asymmetric, and none of them were compatible to normal-mode solutions. The unsteady one-way wave process originated as a marginally stable mode at the impermeable/conducting left-hand wall, traveling horizontally through the box, to be transmitted out through the open and thermally insulated right-hand wall. There is no such cause for a one-way wave process at marginal stability in the present problem, since the normal-mode compatible condition at $x = 0$ serves as symmetry conditions for the eigenfunctions around the z axis.

It is difficult to prove mathematically that the principle of exchange of stabilities is valid, so we argue physically that there is no available cause for it to be violated. Such a cause need asymmetry between two end-walls, where none of the boundary conditions support normal modes. The present problem has one normal-mode compatible wall (with symmetry condition), preventing that a one-way wave can exist at marginal stability. At marginal stability the flow must therefore be steady, and the heat equation (21) then reduces to

$$-w = \nabla^2 \theta. \tag{22}$$

We introduce the streamfunction ψ by the relationships

$$(u, w) = \left(\frac{\partial \psi}{\partial z}, -\frac{\partial \psi}{\partial x} \right), \tag{23}$$

satisfying the continuity equation (11).

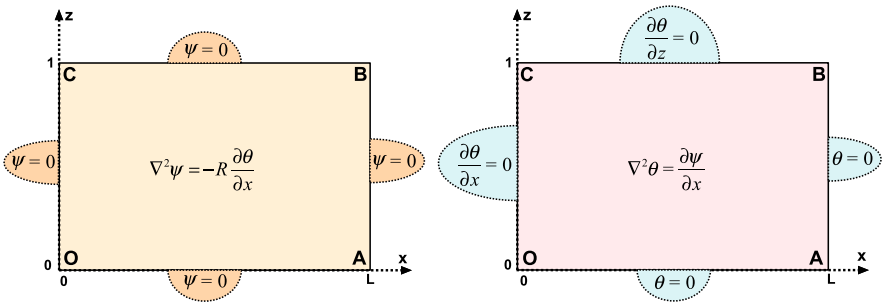

Fig. 1 Illustration of the governing equations and corresponding boundary conditions of the coupled eigenvalue problem.

2.4 The chosen boundary conditions

We first reformulate the above boundary conditions, in terms of the perturbations. The lower boundary is assumed impermeable and perfectly heat conducting

$$\psi = \theta = 0, \quad z = 0, \tag{24}$$

while the upper boundary is impermeable, with constant given heat flux

$$\psi = \frac{\partial\theta}{\partial z} = 0, \quad z = 1. \tag{25}$$

We choose boundary conditions at the two sidewalls. The left hand sidewall is impermeable and thermally insulating

$$\psi = \frac{\partial\theta}{\partial x} = 0, \quad \text{at} \quad x = 0, \tag{26}$$

while the right hand sidewall is impermeable and perfectly heat conducting

$$\psi = \theta = 0, \quad \text{at} \quad x = L. \tag{27}$$

We have here introduced the aspect ratio $L = l/h$, which is the dimensionless width of the porous rectangle.

In *Figure* 1 we present a definition sketch in terms of dimensionless variables. Here the four corners of the rectangle are denoted by O, A, B, C. Their respective coordinates are $(0,0)$, $(L,0)$, $(L,1)$ and $(0,1)$. With the present choice of boundary conditions, the two sides OA and CO can be considered as symmetry lines where the eigenfunctions may be extended as a physically valid flow field on the other side, since they correspond to internal cell walls between two neighboring counter-rotating convection cells. This is is not the case for the two sides AB and BC, beyond which any extrapolations of the mathematical eigenfunctions would not make sense physically.

The local eigenfunction fields at the onset of convection behave differently near each of the four corners. The corner O is the origin, about which the eigenfunctions have local behaviors equivalent to that of the sinusoidal HRL

eigenfunctions, because of the admissible symmetric extrapolations of the local eigenfunctions on both sides close to this corner. The corners A and C allow local analytical description of the eigenfunctions, since a symmetric extrapolation is admissible in one of the two spatial directions around each of these corners. The remaining corner B is the troublesome corner where no extrapolation is legal, and we lack analytical knowledge concerning the local behavior. In the present paper, the numerical solution near the corner B will represent our only information, apart from the boundary conditions that meet in B.

2.5 The coupled differential equations

There are two coupled second-order equations, to be combined with homogeneous boundary conditions for w and θ. We introduce the streamfunction ψ and rewrite the coupling equations between θ and w as

$$\nabla^2\theta = \frac{\partial\psi}{\partial x}, \tag{28}$$

$$\nabla^2\psi + R\frac{\partial\theta}{\partial x} = Z(z), \tag{29}$$

where the unknown function $Z(z)$ is a constant of integration in the x direction. $Z(z)$ may be evaluated at any value of x, and we choose $x = 0$ to find

$$Z(z) = \left(\nabla^2\psi + R\frac{\partial\theta}{\partial x}\right)_{x=0} = \left.\frac{\partial^2\psi}{\partial x^2}\right|_{x=0}, \tag{30}$$

applying the boundary conditions (26). The same condition is applied to the z component of Darcy's law (10), after taking its normal derivative at the wall, giving

$$\left(-\frac{\partial^2\psi}{\partial x^2} + \frac{\partial^2 p}{\partial x\partial z}\right)_{x=0} = R\left.\frac{\partial\theta}{\partial x}\right|_{x=0} = 0. \tag{31}$$

The x component of Darcy's law can be differentiated along the left-hand wall to give

$$\frac{\partial^2 p}{\partial x\partial z} = -\frac{\partial^2\psi}{\partial z^2} = 0, \quad x = 0. \tag{32}$$

Combining these two conditions at $x = 0$ gives what we need to determine $Z(z)$ in eq. (30)

$$Z(z) = \left.\frac{\partial^2\psi}{\partial x^2}\right|_{x=0} = 0, \tag{33}$$

and thereby simplify eq. (29) to

$$\nabla^2\psi + R\frac{\partial\theta}{\partial x} = 0. \tag{34}$$

2.6 An attempt to decouple the eigenvalue problem

In order to analyze this fourth-order eigenvalue problem mathematically, it is an advantage to uncouple the unknown functions $\theta(x,z)$ and $\psi(x,z)$, if possible. The governing equations for the perturbation temperature and streamfunction are easily uncoupled to two equal fourth-order equations

$$\nabla^4\theta + R\frac{\partial^2\theta}{\partial x^2} = 0, \tag{35}$$

$$\nabla^4\psi + R\frac{\partial^2\psi}{\partial x^2} = 0. \tag{36}$$

We will attempt to uncouple the boundary conditions by expressing them by $\theta(x,z)$ alone. If we succeed, it is straightforward to derive the equivalent conditions expressed by $\psi(x,z)$ alone. Thus we try to formulate a purely thermal eigenvalue problem. The conditions at the lower wall OA are easily uncoupled. The heat equation (22) implies that the conditions (24) can be written

$$\theta = \frac{\partial^2\theta}{\partial z^2} = 0, \quad z = 0. \tag{37}$$

The conditions (25) at the upper wall BC can be rewritten as

$$\frac{\partial\theta}{\partial z} = \nabla^2\theta = 0, \quad z = 1, \tag{38}$$

again by the heat equation. The left-hand wall must express equivalence with the internal wall of a normal-mode cell. Manipulating the boundary conditions (26) in combination with the governing equations, these conditions at the left hand wall can be rewritten as

$$\frac{\partial\theta}{\partial x} = \frac{\partial^3\theta}{\partial x\partial z^2} = 0, \quad \text{at} \quad x = 0, \tag{39}$$

thereby expressing a local degeneracy along the side CO where the vorticity is zero. One single boundary remains, which is the right-hand wall AB. However, here the project of decoupling the eigenvalue problem terminates itself. The innocent-looking kinematic condition is $\psi = 0$ at $x = L$, and it implies that all vertical derivatives of ψ are also zero along the wall AB. However, nothing is known about the x derivatives of ψ along the right-hand wall. Without such knowledge, we cannot derive a valid thermal equivalent of the kinematic condition, which was successful for the three other sides of the rectangle $OABC$. We conclude that the complete eigenvalue problem cannot be decoupled, and it must be stated as a coupled problem in the set of eigenfunctions $(\psi(x,z), \theta(x,z))$.

3 The marginal state of convection

The full solution for the marginal state of convection must be found numerically, since no analytical solutions are known for this fourth-order eigenvalue problem without degeneracies in 2D. No Fourier methods are known, but in principle a double power series solution in terms of x and z could be attempted. It would at best converge slowly, so a finite element method is a better alternative. We use the commercial finite-element package Comsol Multiphysics.

Nevertheless we will develop analytical approaches concerning the eigenfunctions in the vicinity of three of the four corners of the porous rectangle.

3.1 Local approximations for the eigenfunctions

We will start with the lower left-hand corner $(0,0)$ and attempt to develop locally valid asymptotic expressions for the eigenfunction in the vicinity of each corner.

3.1.1 Local flow near $(0,0)$

The first corner that we will consider is the origin O, with coordinates $(0,0)$. The local eigenfunctions will here follow the classical HRL solution. With the choice of unity local amplitude for the temperature perturbation, this gives the set of two local eigenfunctions near O

$$\theta = \cos(kx)\sin(mz), \qquad \psi = -\frac{k^2+m^2}{k}\ \sin(kx)\sin(mz), \tag{40}$$

valid asymptotically as $0 < x \ll 1$ and $0 < z \ll 1$, taking care of the governing equations and the local boundary conditions near the corner O. The horizontal and vertical wave numbers (k,m) introduced here, cannot be specified from an analytical point of view, since they do not depend solely on the local boundary conditions along the sides meeting in the corner O. They depend on the full eigenvalue problem, for which no analytical solution is available.

Near the corner $(0,0)$, only the leading terms in each Taylor expansion are representative, giving

$$\theta = mz + O(x^2 z), \quad \psi = -km(k^2+m^2)xz + O(x^3 z) + O(xz^3), \tag{41}$$

to be compared with the numerical solution below.

3.1.2 Local flow near $(L,0)$

The local behavior of the eigenfunctions near the second corner A (with coordinates $(L,0)$) can be deduced from Nilsen and Storesletten (1990), see also Rees and Tyvand (2004b). Their solution has a degeneracy which implies the existence of two different candidates for local solutions, which we call Alternative $A1$ and Alternative $A2$. We will disregard the relative amplitude of the

temperature perturbation versus the streamfunction.

Alternative A1
The first alternative for possible local eigenfunctions around the corner A is

$$\begin{aligned} \theta &\sim \sin(k(x-L))\sin(\alpha(x-L))\sin(mz), \\ \psi &\sim \cos(k(x-L))\sin(\alpha(x-L))\sin(mz). \end{aligned} \tag{42}$$

The local Taylor expansions for eq. (42), representing alternative $A1$, are given by

$$\begin{aligned} \theta &\sim (x-L)^2 z + O((x-L)^2 z^3), \\ \psi &\sim (x-L)z + O((x-L)z^3) + O((x-L)^3 z), \end{aligned} \tag{43}$$

and we note the qualitative difference between the eigenfunctions: The perturbation temperature has zero normal derivative at the wall AB ($x = 0$), while there is a finite vertical velocity along this wall. In the plots below, this alternative will reveal itself by having great distances between neighboring isotherms near the wall AB, since the normal derivative of the temperature tends to zero with the temperature, and there will be a relatively smaller distance between neighboring streamlines near the wall.

Alternative A2
The degeneracy of this local corner problem implies that streamlines and isotherms can be interchanged. Therefore there is a second alternative $A2$ for possible local eigenfunctions around the corner A, given as

$$\begin{aligned} \theta &\sim \cos(k(x-L))\sin(\alpha(x-L))\sin(mz), \\ \psi &\sim \sin(k(x-L))\sin(\alpha(x-L))\sin(mz). \end{aligned} \tag{44}$$

The corresponding local Taylor expansions for eq. (44), representing alternative $A2$, are

$$\begin{aligned} \theta &\sim (x-L)z + O((x-L)z^3) + O((x-L)^3 z) \quad , \\ \psi &\sim (x-L)^2 z + O((x-L)^2 z^3) \qquad\qquad\quad , \end{aligned} \tag{45}$$

which means that Alternative $A2$ interchanges the roles of θ and ψ in Alternative $A1$. Thus the vertical velocity has zero normal derivative at the wall AB ($x = 0$), while there is a finite normal derivative of the temperature perturbation along this wall. In the plots below, this alternative will reveal itself by having a small distance between neighboring isotherms near the wall AB, and a relatively greater distance between neighboring streamlines near the wall.

These one-term local expansions require $|x - L| \ll 1$ and $0 < z \ll 1$. The three wave numbers (k, m, α) that are present in the mathematical solution by Rees and Tyvand (2004b), lose their significance to the leading order of the Taylor series, since they do not affect the shapes of the eigenfunctions. The

degeneracy that is responsible for the two distinct alternatives of eigenfunctions, exist because of the wave number of degeneracy α, which is determined by a Helmholtz equation.

The numerical solution should determine which of the two candidates (42) and (44) for local eigenfunctions near A that are actually represented in the eigenfunctions of marginal stability. In general, a linear combination of these two local solutions is also possible, and it must be considered if none of the two alternatives fit.

3.1.3 On the troublesome corner $(L, 1)$

The local thermomechanical solution near the third corner B (with coordinates $(L, 1)$) will not be discussed from an analytical point of view. B is the troublesome corner, because of the boundary conditions of the two sides that meet there. Both AB and BC have boundary conditions that are incompatible with normal modes. Singularities may arise at corners where there is an encounter of boundary conditions that are mutually in conflict. From a physical point of view, it is not evident whether or not there is a conflict between the homogeneous boundary conditions that meet in B. Such conflicts are more obvious in the presence of non-homogeneous boundary conditions, since the forcing along one boundary may appear as illegal at the meeting point with a perpendicular boundary. A well-known example is the impulsive wavemaker (Peregrine 1972). The singularity of the wavemaker problem is due to the fact that one non-homogeneous boundary condition violates the neighboring homogeneous condition at the waterline corner where the moving wall and the free surface meet. Such a conflict cannot arise in a second-order eigenvalue problem with the Laplace operator subject to homogeneous boundary conditions. This is because a second-order homogeneous problem has only one condition, either of the Dirichlet, Neumann or Robin type. Since one homogeneous boundary condition can always adjust to another homogeneous condition at a corner where the boundaries meet, there will be no resulting singularity.

The situation is different for a fourth-order problem, like the present problem. At each portion of the boundary, there will usually be a pair of two valid boundary conditions, which is the kinematic and the thermal condition in the present physical problem. It is not always possible to make continuous adjustments where one pair of conditions is confronted with another pair of conditions at the common corner where their respective boundaries meet. In general, discontinuities or singularities may therefore occur at a corner where the sets of homogeneous boundary conditions for a fourth-order problem meet one another. A well-known example of this type is the Moffatt vortices (Moffatt 1964), representing a corner singularity for a driven viscous cavity with no-slip condition along the walls. The knowledge of such cases indicates that a corner singularity may exist in our troublesome corner C. Whether or not a singularity may be resolved by an inner expansion is another question, but first one has to identify the singularity with its spatial dependency. The present eigenvalue problem has the additional difficulty that it cannot be uncoupled into

an eigenvalue problem for the temperature alone. Thereby a possible corner singularity in the temperature field will be interwoven with a flow singularity. We do not pursue this difficult topic in the present work.

3.1.4 Local flow near $(0, 1)$

At last we consider the fourth corner C, with coordinates $(0, 1)$. The local eigenfunctions are unique (not degenerate), and the velocity field will have the same local form as it has near the corner O, which is the formula (41). The only modification to be made is the transformation of the local coordinates $z \to (z - 1)$, resulting in the formula

$$\psi \sim x(z-1) + O(x^3(z-1)) + O(x(z-1)^3), \tag{46}$$

valid for the local streamfunction around the corner C. This local flow is irrotational, because the vorticity is zero along the whole side CO, which is a line of symmetry that corresponds to a cell wall. The local irrotational flow around the corner C implies that there is a locally valid complex velocity potential

$$\phi + i\psi \sim (x + i(z-1))^2, \tag{47}$$

valid to the same order of approximation as eq. (46). We have here introduced the imaginary unit i and the real velocity potential ϕ, which is only locally valid because the remaining convection cell is rotational. In order to derive the local temperature field θ, we realize that the isotherms are locally perpendicular to the streamlines, which is implied by the boundary conditions of the two sides BC and CO that meet in the corner C. Thus it follows that

$$\theta = \phi \sim x^2 - (z-1))^2, \tag{48}$$

which is the local perturbation temperature field associated with the streamfunction (46), valid to the same order of approximation around the corner C. According to the local solution (48), there will be an isotherm that meets the corner C at an angle $\pi/4$, which may serve as a check for the numerical solutions below.

3.2 Numerical solution

We have now discussed the four corners of the rectangle, with a warning that there may possibly be a singularity in the corner B. If so, the numerical solution may represent the outer solution in the sense of matched asymptotics, with respect to the corner B. The solution will be well-behaved around the three other corners of the rectangle, where there are no conflicting boundary conditions.

A simple qualitative test of the validity of the numerical solution, is to check that all isotherms are tangential to the sides OA and AB, while all isotherms meet the sides BC and CO at a right angle. In particular, there

must be an isotherm meeting the corner C at an angle of $\pi/4$. The streamlines will have the much simpler behavior of being tangential to all sides of the entire rectangle $OABC$.

The isotherms should be parallel to the side AB but normal to the side BC. This is a switch in behavior around the corner B, that may give a visual test of the accuracy of the numerical solution. An analysis of the vicinity of the corner B is needed to see whether it hides mild singularities in the eigenfunctions. This type of fourth-order eigenvalue problem with the most general Robin-type of homogeneous boundary conditions, is poorly understood mathematically. It is useful to attack these problems numerically before trying to address some of the analytical challenges.

3.2.1 The porous square ($L = 1$)

It is natural to start with the square domain, which is displayed in *Figure* 2. The four eigenfunctions with the lowest Rayleigh numbers are displayed here. The isotherms are represented by solid black lines, supported by color coding. The streamlines are conveniently represented by white graphs on the colored background. There are constant intervals in the displayed values of the perturbation temperature and streamfunction.

A immediate impression from *Figure* 2 is that the link between the cell structure for flow and the cell structure for isotherms is more intricate than what the established literature indicates. There is one full flow cell for the preferred mode (with lowest Rayleigh number) in the horizontal direction, while there is one and a half cell for the isotherms.

The lowest Rayleigh number $R = 36.719$ is slightly below the critical value $R = 4\pi^2$ for the preferred square cell in the classical HRL problem. There are two opposite deviations in the thermal boundary conditions, compared with the HRL conditions. The upper boundary allows buoyancy to be present, which destabilizes the system compared with the HRL problem, while the right-hand wall $x = L$ has the opposite effect of taking away buoyancy. These two opposite thermal effects at the boundaries tend to neutralize one another in a square. Our kinematic conditions are conservative in the sense that they coincide with the HRL conditions.

Two neighboring flow cells are always mutually counter-rotating, because of the continuity of the eigenfunctions. One cannot tell from the eigenfunctions what is a warm thermal domain of upwelling (positive buoyancy) and what is a cold thermal domain of downwelling (negative buoyancy). If a cell wall is curved, this is not due to a positive buoyancy there, since this particular eigenfunction is also valid for negative buoyancy there, changing the sign of the flow amplitude.

3.2.2 A narrow porous domain ($L = 0.5$)

Figure 3 shows the six eigenfunctions with the lowest Rayleigh number for a narrow rectangle with the aspect ratio $L = 0.5$.

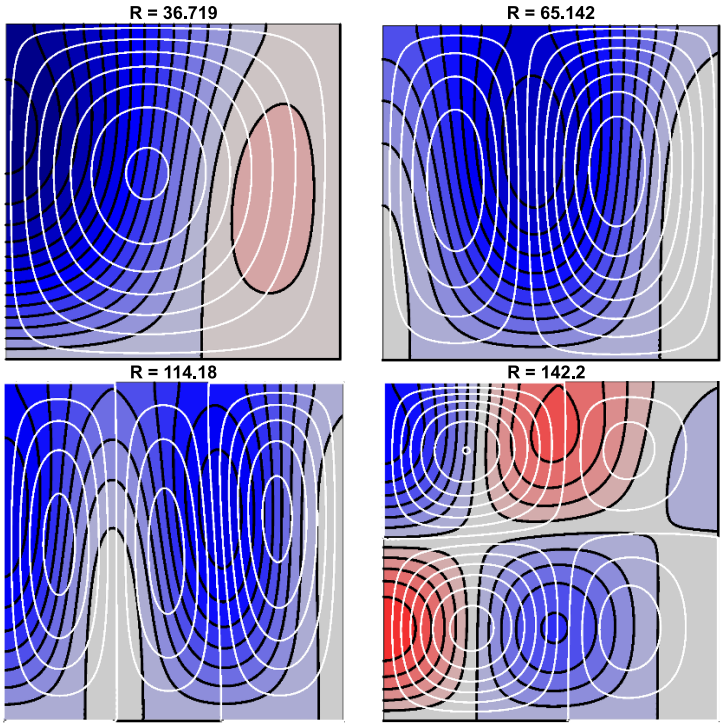

Fig. 2 Isolines for the eigenfunctions at marginal stability for a square $L = 1$. Black lines represent isotherms. White lines represent streamlines.

When L is smaller than one, we expect a greater tendency of multiple cell structures in the vertical direction. Yet the preferred cell with minimum Rayleigh number is always expected to be one single flow cell, and with one dominating thermal cell, with an additional smaller and weaker thermal cell on the right hand side. We see that already the eigenstate with the second lowest Rayleigh number has a double-cell structure in the vertical direction. This is an interesting contrast to the previous case $L = 1$, where the first double-cell structure in the vertical direction appears for the eigenfunctions with the fourth lowest Rayleigh number.

Figure 3 reveals curved cell walls that are not parallel to the boundaries of the rectangle. This is true for cell structures both in the horizontal and the vertical direction. The cell walls are curved both for the thermal eigenfunction and the flow eigenfunction (streamlines).

3.2.3 A moderately wide porous domain ($L = 2$)

The case of infinite width with the present conditions for the lower and upper boundaries, was first studied by Nield (1968, Appendix), who established the

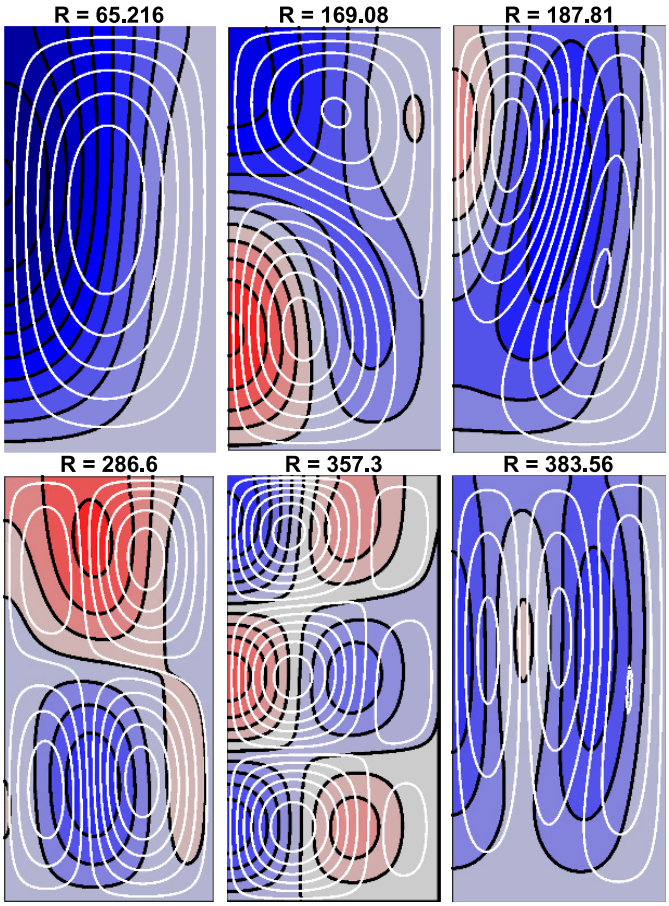

Fig. 3 Isolines for the eigenfunctions at marginal stability for a narrow rectangle with aspect ratio $L = 0.5$. Black lines represent isotherms. White lines represent streamlines.

critical Rayleigh number and wave number

$$Ra_c = 27.10, \quad \alpha_c = 2.33, \tag{49}$$

and these are asymptotic limits expected to be valid as $L \to \infty$. We expect these limit values to be relevant for comparison with the numerical solution when L is significantly greater than one.

Figure 4 shows the six eigenfunctions with the lowest Rayleigh number for a wide rectangle with the aspect ratio $L = 2$. The lowest eigenvalue is $R = 29.676$. It is somewhat greater than the limit value 27.10 for an infinitely wide rectangle, since there is a significant stabilizing effect of the wall AB where buoyancy is taken away due to zero temperature perturbation. There is no precise critical wave number for $L = 2$.

Figure 4 shows only flow cells that do not split in the vertical direction. Thus there are no counter-rotating neighboring cells in the vertical direction,

only in the horizontal direction. With this background, it is remarkable that some of the thermal cells are local and incomplete, not extending throughout the layer, but confined near one of the boundaries, even though there is no locally recirculating flow cell there. This type of intricate relationship between streamlines and isotherms seems to be outside the reach of analytical solutions.

Since *Figure* 4 show cases that comprise two and more full flow cells, we see that the cell width is not constant for the present set of boundary conditions. Constant cell width is usually the case with known solutions for the onset of convection in 2D rectangular boxes, but there is one exception: The rectangular box studied by Rees and Tyvand (2004a), shows a one-way wave with continuously varying wavelength being repeatedly generated at $x = 0$ to be advected out of the porous rectangle at $x = L$. This behavior occurs because of the mutual asymmetry between the thermomechanical conditions at $x = 0$ and those at $x = L$.

A general tendency in all the *Figures* 2-4 is a higher concentration of streamlines than of isotherms near the right-hand side AB of the rectangle. This local structure of the eigenfunctions near the corner A seems to correspond to the alternative $A1$ with the local dependencies given by eq. (45). Alternative $A1$ corresponds to zero normal derivative of the temperature along the boundary where the temperature is also zero, but is only one of two alternatives for the local field around the corner A. If it is correct, it it is not valid along the entire wall AB, but only over a portion of AB close to the corner A. This means that a nonzero temperature gradient normal to the wall is expected along the upper parts of AB near the corner B. This is in fact a general trend in *Figures* 2-4, that the isotherms next to the side AB get gradually closer to this wall as we move along it from A to B.

3.2.4 Critical Rayleigh number as a function of the aspect ratio

Figure 5 presents the Rayleigh number graphs of the 10 lowest onset modes, showing how they vary with aspect ratio L. The graphs for the different eigenfunctions are repeatedly very close to intersecting one another, although close-up views (one example given) reveal that they actually never overlap. Although slowly in most cases, these graphs approach the asymptotic result of 27.10 as $L \to \infty$.

We link *Figure* 5 to *Figures* $2-4$ by marking with circles all the combinations of Rayleigh numbers R and aspect ratios L that are represented in these plots of eigenfunctions.

3.2.5 Wide-rectangle asymptotics for the critical wave number

Generally there is no precise wave number parameter for these non-normal modes of convection onset. That said, we may nevertheless identify an emerging wave number near the left-hand side CO of the rectangle as it gets very wide. *Figure* 6 shows the isotherms and streamlines for the case $L = 4$, where

we display the eigenfunctions for the two lowest onset modes. Only the preferred (lowest) onset mode shows the behavior that we are looking for, approaching the asymptotic critical wave number $\alpha_c = 2.33$ mentioned above. Asymptotically as $L \to \infty$, two vertical cell walls will emerge close to the right-hand side of the semi-infinite rectangle (keeping the side CO fixed along the z axis): First a thermal cell wall located at $x = \pi/(2\alpha_c) = 0.6742$. Next a vertical dividing streamline located at $x = \pi/\alpha_c = 1.3483$, which is an internal flow-cell wall. These two cell walls are not exactly vertical for the finite width $L = 4$, so we have determined numerically their upper and lower points where they meet the boundaries. The exact thermal cell wall for $L = 4$ meets the lower and upper boundary at the points $(0, 0.6683)$ and $(1, 0.6767)$, respectively. The exact flow cell wall for $L = 4$ meets the lower and upper boundary at the points $(0, 1.3315)$ and $(1, 1.3282)$, respectively. This is in good agreement with the asymptotic results derived from Nield (1968), and as expected, the thermal cell wall will be the one that is closest to vertical, simply because it is the cell wall that is the closest neighbor to the left-hand boundary of the porous rectangle. The critical Rayleigh number is 27.749, which is two percent above the asymptotic limit value 27.10 from Nield (1968).

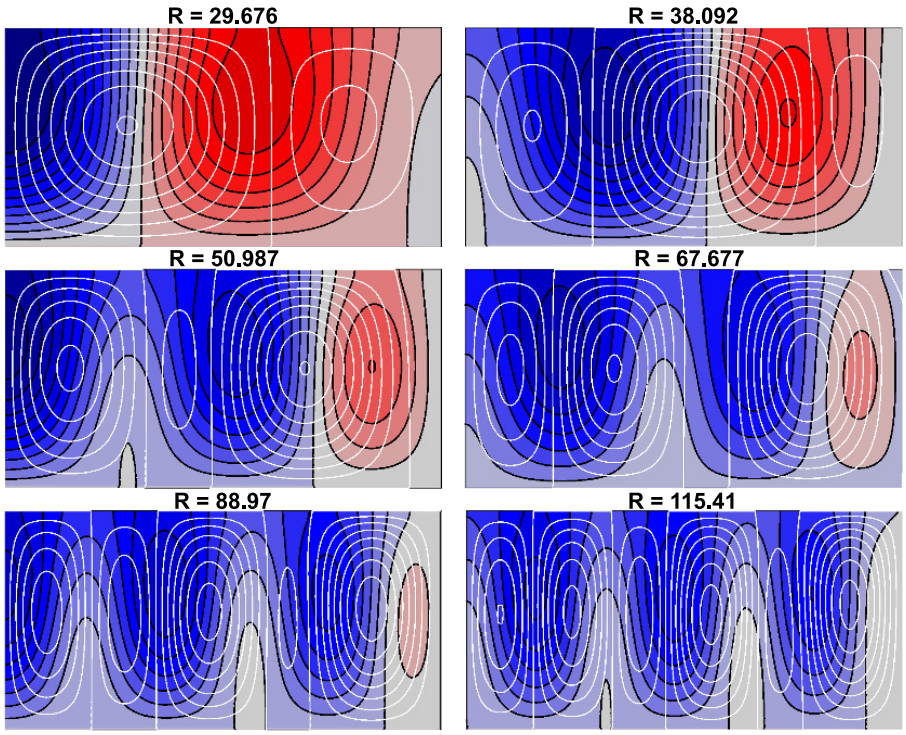

Fig. 4 Isolines for the eigenfunctions at marginal stability for a wide rectangle with aspect ratio $L = 2$. Black lines represent isotherms. White lines represent streamlines.

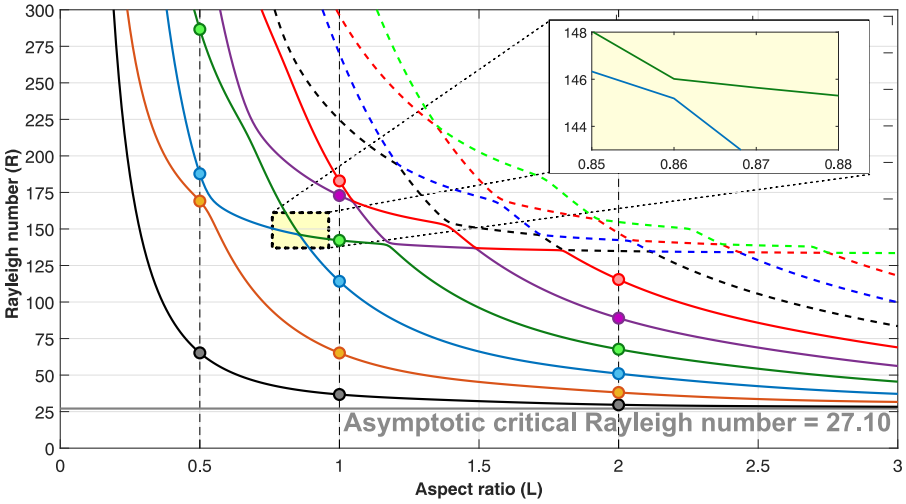

Fig. 5 Rayleigh numbers (R) at marginal stability as a function of aspect ratio (L) for the 10 first eigenfunctions. The filled circles refer to the cases displayed in *Figures* $2-4$.

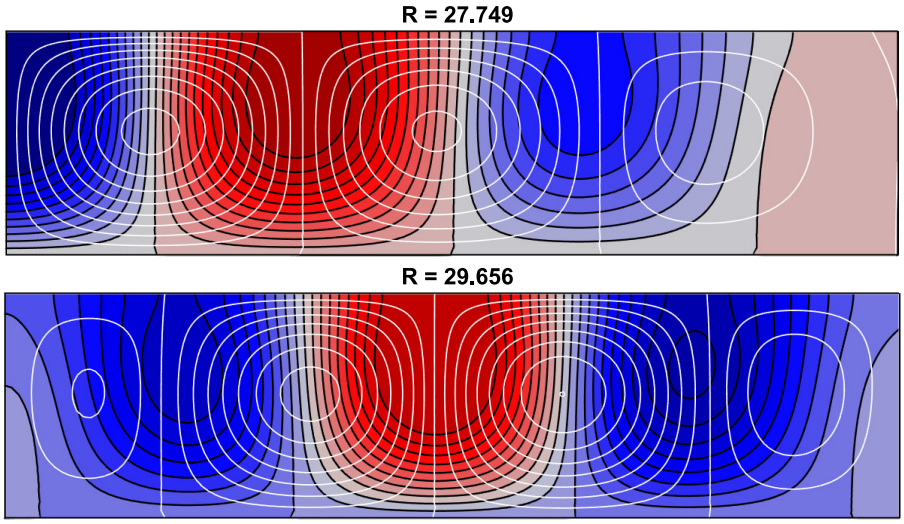

Fig. 6 Isolines for the eigenfunctions at marginal stability for a wide rectangle with aspect ratio $L = 4$. Black lines represent isotherms. White lines represent streamlines.

4 Discussion and outlook

The general mathematical theory of fourth-order eigenvalue problems is not highly developed, in great contrast to the deep established insights into har-

monic analysis of second-order problems. The Darcy-Bénard problem of convection onset in porous enclosures is therefore of basic mathematical and physical interest, since it is one of the simplest fourth-order eigenvalue problems of dissipative processes. This is a thermomechanical instability problem where entropy is being produced by a steady thermal process in the basic state, and where thermal as well as mechanical entropy-producing processes occur in any disturbed state.

The present results are solely numerical, apart from the locally valid leading-order Taylor series solutions that we developed near three of the four corners of the rectangle. These numerical eigenfunctions contain several novel features that we hope will stimulate more research on this topic, which is a well-established one since the pioneering work by Horton and Rogers (1945). From the early work, one is used to think that the cells for the flow (closed-streamline structures) and the cells for the temperature field, are essentially linked together with a mutual phase shift of a quarter of a wavelength horizontally. This fixed spatial phase shift is easy to interpret physically, for two reasons: (1) An upwelling domain at a cell boundary with zero horizontal flow corresponds naturally to a maximal temperature perturbation occurring in the middle of a thermal cell. (2) In the middle of a flow cell, where the vorticity and the horizontal velocity is maximal, no buoyancy is active, which means that there is a thermal cell wall of zero perturbation temperature.

Rees and Tyvand (2004b) showed that this quarter of a wavelength displacement between internal cell walls for flow and cell walls for temperature holds for a class of 2D enclosures, with arbitrary contours that are impermeable and have zero perturbation temperature. However, this strict and precise relationship between streamlines and isotherms appears to rest on some degeneracy in the eigenvalue problem. We have now demonstrated that a full non-normal mode behavior in 2D, dictated by properly chosen homogeneous thermomechanical boundary conditions, makes the relationship between streamlines and isotherms much more complicated. There is no such thing as a fixed spatial phase shift between thermal cell walls and cell walls of recirculation.

At the left-hand wall, there is a cell wall for the streamlines, while this wall cuts halfway through a temperature cell. At the right-hand wall, however, both the streamlines and the temperature field have a joint cell wall. This indicates that the number of temperature cells will always be half a cell more than the number of streamline cells, or opposite. Rees and Tyvand (2004b) showed that the streamlines and isotherms could have been interchanged for the present problem, if there had been a normal-mode solution in the vertical direction, because of a degeneracy in that eigenvalue problem. As a contrast, the present problem has no degeneracy, and our numerical results indicate that there are always half a cell more temperature cells than flow cells, even though the counting of temperature cells is difficult because many of these cells do not form closed curves within the porous rectangle. As a contrast, all the flow cells are closed, which is a trivial fact following from our requirement that the boundary of the rectangle is a streamline.

There are curved cell walls, both for the internal flow cells and the cells for the perturbation temperature. This cannot occur in a rectangle with normal-mode compatible boundary conditions in at least one spatial direction. There are no symmetries in our chosen thermomechanical conditions along the four sides of the rectangle. This lack of internal symmetries within a rectangle is sufficient to achieve complicated cell structures with curved cell walls, even in linear theory. One is used to think that such complicated cell structures can only be due to nonlinear effects, but this is not true because of the hidden complexities in the linearized problem in its general formulation for a porous cavity of finite extent. In the literature, a tacit preference for normal-mode compatible boundary conditions seems to have granted degenerate classes of eigenfunctions an artificially high status as solutions for convection onset in porous rectangles. The present paper shows the importance of establishing a broader view on the eigenfunctions of marginal stability in porous media heated from below. In a field which has reached the maturity of Darcy-Bénard convection, it can no longer be defended to let the physical perspective of linear theory be guided by mathematical convenience.

In the present work, we have investigated the local flows around three of the four corners of the rectangle, where the eigenfunctions are continuous. There is a possible singularity at the fourth corner, around which we are unable to find a local solution. We leave for later work the properties of the eigenfunctions near this troublesome corner, noting that the thermomechanical conditions along both sides meeting in this corner are incompatible to normal modes. The numerical solution is well-behaved along the boundaries except for a domain close to the single corner where there is no local solution. This indicates that the solution that we have found numerically represents an outer solution in a matched asymptotic expansion. The validity of this outer solution is important for determining uniquely the critical Rayleigh number for the onset of convection. The Rayleigh numbers that we have computed, look physically plausible to the extent that they have been compared with existing results. The critical Rayleigh number is an integrated quantity that should not be affected by a weak corner singularity.

References

Barletta, A. and Storesletten, L. (2015) Onset of convection in a vertical porous cylinder with a permeable and conducting side boundary. Int. J. Therm. Sci. **97**, 9-16.

Beck, J.L. (1972) Convection in a box of porous material saturated with fluid. Phys. Fluids **15**, 1377-1383.

Haugen, K.B. and Tyvand, P.A. (2003) Onset of thermal convection in a vertical porous cylinder with conducting wall. Phys. Fluids **15**, 2661-2667.

Horton, C.W. and Rogers, F.T. (1945) Convection currents in a porous medium. J. Appl. Phys. **16**, 367-370.

Lapwood, E.R. (1948) Convection of a fluid in a porous medium. Proc. Camb.

Phil. Soc. **44**, 508-521.

Lyubimov, D.V. (1975) Convective motions in a porous medium heated from below. J. Appl. Mech. Tech. Phys. **16**, 257-261.

Moffatt, H.K. (1964) Viscous and resistive eddies near a sharp corner. J. Fluid Mech. **18**, 1-18.

Nield, D.A. (1968) Onset of thermohaline convection in a porous medium. Water Resources Res. **11**, 553-560.

Nilsen, T. and Storesletten, L. (1990) An analytical study on natural convection in isotropic and anisotropic porous channels. ASME J. Heat Transf. **112**, 396-401.

Peregrine, D. H. (1972) Flow due to a vertical plate moving in a channel. Unpublished note.

Rees, D.A.S. and Tyvand, P.A. (2004a) Oscillatory convection in a two-dimensional porous box with asymmetric lateral boundary conditions. Phys. Fluids 16, 3706-3714 (2004)

Rees, D.A.S. and Tyvand, P.A. (2004b) The Helmholtz equation for convection in two-dimensional porous cavities with conducting boundaries. J. Eng. Math. 490, 181-193 (2004)

Storesletten, L. and Tveitereid (1991) Natural convection in a horizontal porous cylinder. Int. J. Heat Mass Transf. 34, 1959-1968.

Tyvand, P.A. and Storesletten, L. (2018) Degenerate onset of convection in vertical porous cylinders. J. Eng. Math. 113, 165-181.

Wang, C.Y. (1998) Onset of natural convection in a fluid-saturated porous medium inside a cylindrical enclosure heated by constant flux. Int. Commun. Heat Mass Transfer **25**, 593 - 598.

Wang, C.Y. (1999) Thermo-convective stability of a fluid-saturated porous medium inside a cylindrical enclosure - Permeable top constant flux heating. Mech. Res. Commun. **26**, 603 - 608.

Wooding, R.A. (1959) The stability of a viscous liquid in a vertical tube containing porous material. Proc. R. Soc. Lond. **A252**, 120-134.

Zebib, A. (1978) Onset of natural convection in a cylinder of water saturated porous media. Phys. Fluids **21**, 699-700.